

Geometric properties of two-dimensional critical and tricritical Potts models

Youjin Deng,¹ Henk W. J. Blöte,^{1,2} and Benard Nienhuis³

¹*Faculty of Applied Sciences, Delft University of Technology, P.O. Box 5046, 2600 GA Delft, The Netherlands*

²*Lorentz Institute, Leiden University, P.O. Box 9506, 2300 RA Leiden, The Netherlands*

³*Institute of Theoretical Physics, University of Amsterdam, Valckenierstraat 65, 1018 XE Amsterdam, The Netherlands*

(Received 23 October 2003; published 27 February 2004)

We investigate geometric properties of the general q -state Potts model in two dimensions, and define geometric clusters as sets of lattice sites in the same Potts state, connected by nearest-neighbor bonds with variable probability p . We find that, besides the random-cluster fixed point, both the critical and the tricritical Potts models have another fixed point in the p direction. For the critical model, the random-cluster fixed point p_r is unstable and the other point $p_g \geq p_r$ is stable; while p_r is stable and $p_g \leq p_r$ is unstable at tricriticality. Moreover, we show that the fixed point p_g of a critical and tricritical q -state Potts models can be regarded to correspond to p_r of a tricritical and critical q' -state Potts models, respectively. In terms of the coupling constant of the Coulomb gas g , these two models are related as $gg' = 16$. By means of Monte Carlo simulations, we obtain $p_g = 0.6227(2)$ and $0.6395(2)$ for the tricritical Blume-Capel and the $q=3$ Potts model, respectively, and confirm the predicted values of the magnetic and bond-dilution exponents near p_g .

DOI: 10.1103/PhysRevE.69.026123

PACS number(s): 05.50.+q, 64.60.Cn, 64.60.Fr, 75.10.Hk

I. INTRODUCTION

The geometric description of fluctuations near a critical point has been the subject of a long history, which goes back to the formulation of phase transitions in terms of the droplet model [1]. For the general q -state Potts model [2,3], the critical singularities can be represented in terms of Kasteleyn-Fortuin (KF) clusters [4,5]. For clarity, we start from the Hamiltonian of the q -state Potts model on the square lattice:

$$\mathcal{H}/k_B T = -K \sum_{\langle i,j \rangle} \delta_{\sigma_i, \sigma_j} \quad (\sigma = 1, 2, \dots, q), \quad (1)$$

where the sum is over all nearest-neighbor (NN) sites and K is the coupling strength. This model can be exactly mapped onto a random-cluster model [4]. Between each pair of NN sites, a bond is placed with the probability $p = 1 - \exp(-K)$, so that the whole lattice is decomposed into connected clusters, i.e., the aforementioned KF clusters. The statistical weight of each bond-variable configuration is expressed by the partition sum of the random-cluster model as

$$Z(q; K) = \sum_b v^{n_b} q^{n_c} \quad (v = e^K - 1). \quad (2)$$

The sum is over all bond-variable configurations, and n_b and n_c are the total numbers of bonds and KF clusters, respectively.

The partition sum (2) defines the general Potts model with noninteger $q \geq 0$, which has a continuous and a first-order phase transition for $0 \leq q \leq 4$ and for $4 < q$, respectively. Near the critical point $K_c(q)$, the distribution of KF clusters reflects critical singularities of the Potts model (1). For instance, the scaling properties of the average size of critical KF clusters are determined by the magnetic exponent $X_h(q)$. Exact values of $X_h(q)$ have already been obtained by the theory of the Coulomb gas [6,7], and are also included

within the predictions of the conformal field theory [8,9]. In terms of the coupling constant of the Coulomb gas g , $X_h(g)$ is expressed as

$$X_h(g) = \frac{(g-2)(6-g)}{8g}, \quad (3)$$

where g is related to q as $q = 2 + 2 \cos(g\pi/2)$ with $2 \leq g \leq 4$ for the critical branch of the Potts model [6,7].

Apart from KF clusters, so-called Potts clusters [10–13] have received considerable attentions, which are defined as sets of NN sites in the same Potts state. Thus, bonds are *always* present between any pair of NN sites as long as they are occupied by the same Potts variable. For critical Potts model (1), the exponents for the Potts clusters are generally different from those for the KF clusters. A well-known example is the Ising model ($q=2$). The exponent for the Ising clusters, i.e., the $q=2$ Potts clusters, is $X_h^{(p)} = 5/96$, [10,11,13] equal to the magnetic exponent of the tricritical $q=1$ Potts model. Here, the superscript (p) refers to the Potts clusters. For the bond percolation model ($q=1$), all lattice sites belong to the same Potts cluster, and thus $X_h^{(p)}(q=1) = 0$. Apparently, $X_h^{(p)}(q) \neq X_h(q)$ in these cases. Within the predictions of the conformal field theory, Vanderzande [12] interpreted $X_h^{(p)} = 7/80$ and $1/8$ for the critical $q=3$ - and 4-state Potts models, respectively. However, for the general noninteger $0 \leq q \leq 4$ Potts model, exact value of $X_h^{(p)}$ has not been reported yet, as far as we know. This is one purpose of the present paper.

The tricritical Potts model [3] can be obtained by including vacancies in the “pure” Potts model (1). The question then arises, what critical exponents describe Potts clusters of the general tricritical q -state Potts model. From Refs. [10–13], it is known that, for the critical Potts model, the exponent $X_h^{(p)}$ approaches the magnetic exponent X_h as q increases. Particularly, $X_h^{(p)} = X_h$ for $q=4$. Since the tricritical branch of the Potts model is an extension of the critical Potts

model [3], we simply assume that, for the tricritical Potts model, the Potts clusters and the KF clusters are described by the same critical exponents. This will be confirmed numerically later.

Moreover, for both the critical and the tricritical Potts models, we investigate a general type of “geometric” clusters, which are defined analogously as the aforementioned KF clusters, but the bond probability can have a variable value $0 \leq p \leq 1$. Thus, KF and Potts clusters are just the special cases of geometric clusters with $p = 1 - \exp(-K)$ and 1, respectively. For the critical Potts model, it is generally believed that, in terms of geometric clusters, the percolation threshold p_g coincides with the critical point of the corresponding Potts model or random-cluster model p_r , i.e., $p_g = p_r = 1 - \exp(-K_c)$. In the contrast, at tricritical points K_{tc} , we show that the percolation threshold p_g does not coincide with $p_r = 1 - \exp(-K_c)$, but $0 < p_g < p_r$. Furthermore, critical exponents near p_g are different from those near p_r . On the basis of the theory of the Coulomb gas, we predict values of critical exponents near p_g for the tricritical q -state Potts model.

To confirm these predictions, we perform Monte Carlo simulations for the tricritical Blume-Capel [14,15] and the $q=3$ Potts model [3]. Numerical data clearly demonstrate the existence of p_g for the tricritical Potts model, and confirm the predicted critical exponents.

The organization of the present paper is as follows. In Sec. II, we outline a general theory and do several predictions for the critical and the tricritical branches of the Potts model. Section III presents our Monte Carlo investigation, which confirms the predictions in Sec. II. Then, a short discussion is given in Sec. IV.

II. GENERAL ANALYSIS

We start from the critical Potts model, described by Eq. (1). For this model, the statistical properties of geometric clusters can be obtained from a “mixed” Potts model [5,16] with the Hamiltonian

$$\mathcal{H}/k_B T = -J \sum_{\langle i,j \rangle} (\delta_{\tau_i, \tau_j} - 1) \delta_{\sigma_i, \sigma_j} - K \sum_{\langle i,j \rangle} \delta_{\sigma_i, \sigma_j} \quad (4)$$

The second term is just the aforementioned pure q -state Potts Hamiltonian (1); the first term contains auxiliary Potts variables $\tau = 1, 2, \dots, s$, and controls the distribution of bond variables. One can express the partition sum of Eq. (4) in bond variables, and differentiate the resulting free energy with respect to the parameter s . Taking the limit $s \rightarrow 1$, one obtains the distribution of geometric clusters with bond probability $p = 1 - \exp(-J)$. Particularly, if one chooses $J = K$, Hamiltonian (4) assumes a simple form and describes the random-cluster model (2).

For this mixed Potts model (4), the renormalization-group (RG) flow is sketched in Fig. 1(a) in the parameter space (p, K) with $p = 1 - \exp(-J)$. The dashed line represents the random-cluster model with $J = K$. At the critical point $K = K_c$, in terms of geometric clusters, the percolation threshold is just $p_r = 1 - \exp(-K_c)$. Thus, p_r can be considered as a

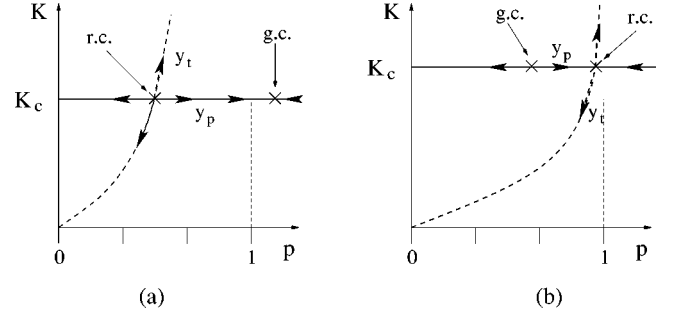


FIG. 1. RG flows of Potts models in the parameter space (K, p) . (a) and (b) apply to the critical and the tricritical Potts models, respectively. The dashed lines represent the random-cluster model $p = 1 - \exp(-K)$. The points “r.c.” and “g.c.” represent the random- and the geometric-cluster fixed points p_r and p_g , respectively. Arrows show the direction of the RG flows.

fixed point in the space (p, K) , which is unstable both in the bond-probability direction p and along the dashed line $J = K$. The scaling properties in these two directions are described by the bond-dilution and the thermal scaling field, respectively. We shall denote their associated exponents as y_p and y_t , respectively, where y_p is also referred to be the red-bond exponent [17].

Near the random-cluster fixed point p_r , exact values of the bond-dilution and the thermal exponents y_p and y_t have already been obtained by various methods. For instance, on the basis of the theory of the Coulomb gas, it has been derived [11,13,17] that the scaling dimensions $X_p = 2 - y_p$ and $X_t = 2 - y_t$ satisfy

$$X_p(g) = \frac{1}{8g} (3g - 4)(g + 4) \quad (5)$$

and

$$X_t(g) = \frac{6 - g}{g}, \quad (6)$$

respectively, where g is the coupling constant of the Coulomb gas, as mentioned before. Furthermore, for integers $0 \leq q \leq 4$, $X_p(q)$ and $X_t(q)$ are also included in the predictions of the conformal field theory. For clarity, we start from the Kac formula describing scalar observables [8,9]

$$X_{i,j}(q) = \frac{[im - j(m+1)]^2 - 1}{2m(m+1)} \quad (m \geq 1), \quad (7)$$

where the positive integer m is related to the conformal analogy c as $c = 1 - 6/m(m+1)$. For the critical branch of the Potts model, one has $\sqrt{q} = 2 \cos[\pi/(m+1)]$. It is known that $X_p(q)$ and $X_t(q)$ can be identified as $X_{i,j}$ with coordinates $(i=0, j=2)$ and $(i=2, j=1)$, respectively. We also mention that the aforementioned magnetic exponent $X_h(q)$ can be interpreted as $X_{i,j}$ with $i=j=(m+1)/2$.

For the critical Potts model ($2 \leq g \leq 4$), Eq. (5) yields $X_p(q) \leq 2$, which indicates that the bond-dilution field is relevant at the random-cluster fixed point p_r , as shown in Fig. 1(a). Thus, geometric clusters at p_r , i.e., KF clusters, and

TABLE I. The bond-dilution and the magnetic exponents X_p and X_h for the two-dimensional Potts model. The superscripts (r) and (g) represent the random- and the geometric-cluster fixed points, p_r and p_g , respectively. The coupling constant of the Coulomb gas is denoted as g , and the positive integer m is related to the conformal anomaly c as $c = 1 - 6/m(m + 1)$.

	Random-cluster fixed point					Geometric-cluster fixed point					
	$q^{(r)}$	$g^{(r)}$	$m^{(r)}$	$X_p^{(r)}$	$X_h^{(r)}$	$X_p^{(g)}$	$X_h^{(g)}$	$m^{(g)}$	$g^{(g)}$	$q^{(g)}$	
Critical	0	2	1	3/4	0	15/4	-3/16	1	8		Tri
	1	8/3	2	5/4	5/48	35/12	0	2	6	0	crit
	2	3	3	35/24	1/8	21/8	5/96	3	16/3	1	ical
	3	10/3	5	33/20	2/15	143/60	7/80	5	24/5	2 + 2 cos(2π/5)	
	4	4	∞	2	1/8	2	1/8	∞	4	4	
Tri	3	14/3	6	65/28	2/21	143/84	15/112	6	24/7	2 + 2 cos(2π/7)	Crit
crit	2	5	4	99/40	3/40	63/40	21/160	4	16/5	2 + 2 cos(2π/5)	ical
ical	1	16/3	3	21/8	5/96	35/24	1/8	3	3	2	
	0	6	2	35/12	0	5/4	5/48	2	8/3	1	

those with the bond-probability $p \neq p_r$ are described by different exponents. For $p < p_r$, we expect that the behavior of geometric clusters is dominated by the trivial $p = 0$ fixed point; while geometric clusters with $p > p_r$, including Potts clusters, are described by a stable fixed point $p_g > p_r$, shown in Fig. 1(a). For later convenience, we shall refer to the point p_g as the geometric-cluster fixed point. For the case of the Ising model on the square lattice, it has been found [13] that $p_g \approx 1.08$, in an unphysical region.

The above discussions apply to the critical branch of the Potts model. For the tricritical Potts model, it is already known [6,7] that the magnetic and thermal exponents $X_h(q)$ and $X_t(q)$ are still given by Eqs. (3) and (6), respectively, but with the coupling constant in the range $4 \leq g \leq 6$. Accordingly, for integers $0 \leq q \leq 4$, $X_t(g)$ and $X_h(g)$ can be interpreted as $X_{1,2}$ and $X_{m/2,m/2}$ in the Kac formula (7), respectively. On this basis, for the tricritical Potts model, we simply assume that the bond-dilution exponent $X_p(q)$ is still given by Eq. (5) with $4 \leq g \leq 6$, and thus corresponds to $X_{2,0}$ in the Kac formula (7).

To distinguish the critical and the tricritical branches of the Potts model, later we shall express critical exponents as a function of g only. Table I lists values of g , $X_p(g)$, and $X_h(g)$ for the Potts model with integer $0 \leq q \leq 4$.

As mentioned earlier, for the critical Potts model, the point p_r is a fixed point in the parameter space (p, K) . Here, we assume that this statement still holds for the tricritical Potts model ($4 < g \leq 6$). Equation (5) yields $X_p(g) > 2$, so that the bond-dilution scaling field is irrelevant near the random-cluster fixed point p_r . On the other hand, it is obvious that the trivial $p = 0$ fixed point is stable. On this basis, we expect that, in the p direction, an unstable fixed point p_g occurs in the range $0 \leq p \leq p_r$ for the tricritical Potts model. We shall also refer to this unstable point p_g as the geometric-cluster fixed point. As far as we know, the existence of p_g has not yet been reported. The expected RG flow is shown in Fig. 1(b), which will be confirmed numerically later.

In conclusion, according to the predicted values of the bond-dilution exponent X_p [11,13,17], we predict that both the critical and the tricritical Potts models have a pair of fixed points p_r and p_g on the critical line parametrized by the

bond probability p . For the critical branch of the Potts model, the random-cluster fixed point p_r is unstable and the geometric-cluster fixed point $p_g > p_r$ is stable. In the contrast, for the tricritical Potts model, p_r is stable and $p_g < p_r$ is unstable. The $q = 4$ Potts model is a marginal case, and these two fixed points p_r and p_g merge together. In the parameter space (p, q) , we illustrate the RG flows in Fig. 2.

The question arises what values the critical exponents take near the geometric-cluster fixed point p_g for the general critical and tricritical Potts model. For the Ising model ($q = 2$), it is already known [10–13] that the fixed point p_g corresponds to p_r of the tricritical $q = 1$ Potts model. In other

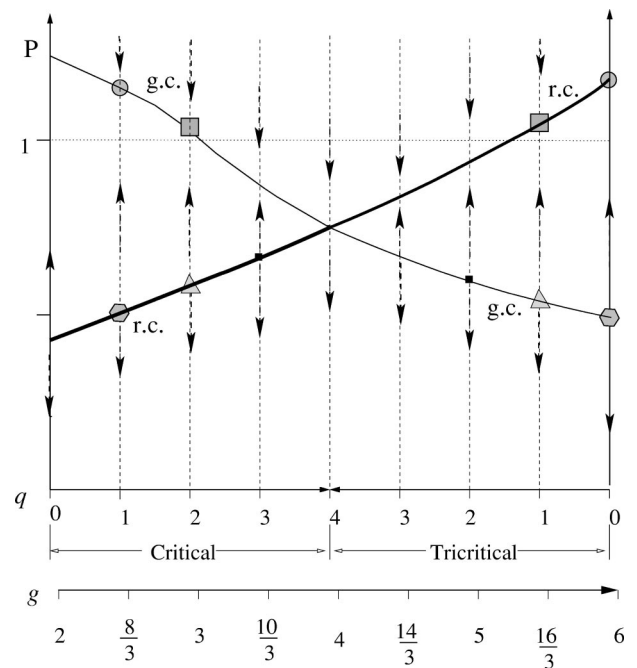


FIG. 2. RG flows in the plane (q, p) for the general q -state Potts model in two dimensions. The thick and thin solid lines represent the random- and the geometric-cluster fixed points p_r and p_g , respectively. Those pairs of points in the same symbol have the same conformal anomaly. Arrows show the direction of the RG flows. The $q = 4$ Potts model is a marginal case.

words, p_g of the tricritical $q=1$ Potts model corresponds to p_r of the Ising model. On this basis, we assume the followings for the general Potts model with $0 \leq q \leq 4$.

Assumption 1. the geometric-cluster fixed point p_g of a critical (tricritical) q -state Potts model corresponds to the random-cluster fixed point p_r of a tricritical (critical) q' -state Potts model.

Assumption 2. the critical q - and tricritical q' -state Potts models have the same conformal anomaly and thus the number m .

For the critical and the tricritical branches of the Potts model, as is well known, the coupling constant of the Coulomb gas g is related to m as $g=4m/(m+1)$ and $g'=4(m'+1)/m'$, respectively. Therefore, the aforementioned two models are related by $gg'=16$.

With these assumptions, critical exponents can be easily obtained for the fixed point p_g . As an example, we consider the magnetic exponent $X_h^{(g)}$ for a model with the coupling constant g . As mentioned earlier, X_h is given by Eq. (3), so that, after the substitution $g=16/g'$, $X_h^{(g)}(g)$ follows as

$$X_h^{(g)}(g) = \frac{(8-g)(3g-8)}{32g}. \quad (8)$$

The same procedure applies to other critical exponents, and the resulting values are consistent with the existing predictions for the critical Potts model with $q=1, 2, 3$, and 4. For clarity, we list values of $X_h^{(g)}$ and $X_p^{(g)}$ in Table I for integer $0 \leq q \leq 4$.

III. MONTE CARLO INVESTIGATION

To confirm the predictions in Sec. II, we perform Monte Carlo simulations for the tricritical Blume-Capel and $q=3$ Potts models.

Tricritical Blume-Capel model. The Ising model with vacancies, also called the Blume-Capel model [14,15], is defined on the square lattice, with the Hamiltonian

$$\mathcal{H}/k_B T = -K \sum_{\langle i,j \rangle} \sigma_i \sigma_j + D \sum_k \sigma_k^2 \quad (\sigma=0, \pm 1). \quad (9)$$

The vacancies are denoted as $\sigma=0$, and D is the chemical potential of the Ising spins $\sigma=\pm 1$. We mention that, in this case, the bond probability for KF clusters is $p=1-\exp(-2K)$.

For $D \rightarrow -\infty$, the vacancies are excluded, and the model reduces to Onsager's spin- $\frac{1}{2}$ model [18]. The critical coupling constant K_c is an increasing function of the chemical potential D , and the critical line $K_c(D)$ terminates at a tricritical point. By means of a sparse transfer matrix technique, we have determined the tricritical point [19] as $K_{tc}=1.6431759(1)$, $D_{tc}=3.2301797(2)$, and $\rho_{tc}=0.4549506(2)$ for the vacancy density. The precision improves significantly over that of the existing results [20], $K_{tc}=1.64(1)$, $D_{tc}=3.22(2)$, and is considered to be sufficient for our present investigation.

For this model (9), however, no cluster Monte Carlo method to flip between vacancies and Ising spins is generally

available. Thus, during the simulations, we fixed the total number of vacancies in order to avoid the critical slowing down due to fluctuations in the number of vacancies. This was realized by a recently developed geometric cluster algorithm [21,22], which moves groups of vacancies and Ising spins on the lattice in accordance with the Boltzmann distribution. A detailed account of the geometric cluster method can be found in Refs. [21,22].

The Monte Carlo simulations were performed at the tricritical point. For finite systems, however, the total number of vacancies V at tricriticality is generally not an integer, so that the actual simulations took place at $V_-=[V_{tc}]=[\rho_{tc} L^2]$ and $V_+=[V_{tc}]+1$, where square brackets $[]$ denote the integer part of the number in it. For a sampled quantity A , its value A_{tc} at the tricritical point is approximated as

$$A_{tc} = \frac{A_+(V_{tc}-V_-)+A_-(V_+-V_{tc})}{V_+-V_-}, \quad (10)$$

and the statistical error margin of A_{tc} is taken as

$$\delta A_{tc} = \frac{1}{V_+-V_-} \sqrt{[\delta A_+(V_{tc}-V_-)]^2 + [\delta A_-(V_+-V_{tc})]^2}. \quad (11)$$

Since we are interested in geometric properties of the Blume-Capel model, the aforementioned geometric clusters have to be constructed with bond probability $0 \leq p \leq 1$ during the sampling procedure. This was realized by a Swendsen-Wang-like algorithm [23]. For a bond- and vacancy-variable configurations, we denote the total number of geometric clusters for as N_c , and the size of the i th cluster as s_i . The following quantities were sampled:

$$S_2 = \frac{1}{L^2} \left\langle \sum_i^{N_c} s_i^2 \right\rangle, \quad S_4 = \frac{1}{L^4} \left\langle \sum_i^{N_c} s_i^4 \right\rangle,$$

and

$$r = \langle S_2 \rangle^2 / \langle S_4 \rangle. \quad (12)$$

It can be easily shown that, at the random-cluster fixed point p_r , the quantity S_2 is just the magnetic susceptibility, and the dimensionless ratio as r plays a role as the universal Binder cumulant [24] in the Potts model.

Periodic boundary conditions were applied, and near the random-cluster fixed point $p_r=1-\exp(-2K_{tc}) \approx 0.96260999$, the system sizes were taken in the range $8 \leq L \leq 120$. Figure 3 shows parts of the Monte Carlo data of the dimensionless ratio r , in which the slope of r decreases as the system size L increases. This indicates that the bond-dilution exponent y_p is a negative number, and thus the random-cluster fixed point p_r is stable, as expected. Moreover, according to the least-square criterion, we fitted the following equation to the data of r :

$$\begin{aligned} r = & r_0 + r_1(p-p_c)L^{y_p} + r_2(p-p_c)^2L^{2y_p} + \dots + r_6(p \\ & - p_c)^6L^{6y_p} + b_1L^{y_1} + b_2L^{y_2} + b_3L^{y_3} + c_1(p-p_c)L^{y_1+y_p} \\ & + n_1(p-p_c)^2L^{y_p}. \end{aligned} \quad (13)$$

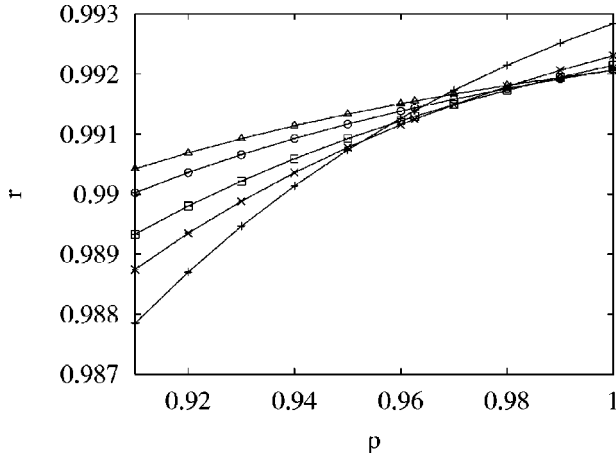


FIG. 3. The dimensionless ratio r near the random-cluster fixed point p_r for the tricritical Blume-Capel model. The data points $+$, \times , \square , \circ , and \triangle represent $L=8, 12, 16, 24$, and 32 , respectively.

Here, the amplitudes r_i , b_i , c_i , and n_i are unknown parameters, and the term with n_1 accounts for the fact that the bond-dilution scaling field is a nonlinear function of $(p - p_c)$. The terms with b_i describe finite-size corrections, and the associated exponents were simply taken as integer numbers as $y_1 = -1$, $y_2 = -2$, and $y_3 = -3$. Furthermore, we fixed p_c at the random-cluster fixed point $p_r \approx 0.96260999$. After a cutoff for small system sizes $L \leq 10$, we obtain $y_p = -0.48(2)$, in agreement with the prediction $y_p = -19/40$ (Table I).

According to Fig. 1(b), for tricritical systems, Potts and KF clusters are described by the same critical exponent, i.e., $X_h^{(p)} = X_h$. Thus, we fitted the following equation to the data of S_2 for Potts clusters:

$$S_2 = L^{-2X_h}(a_0 + a_1 L^{y_1} + a_2 L^{y_2} + a_3 L^{y_3}). \quad (14)$$

Here, the leading finite-size effect arises from the bond-dilution field, so that we set $y_1 = y_p = 2 - X_p = -19/40$, $y_2 = 2y_1 = -19/20$, and $y_3 = -2$. After a cutoff for small system sizes $L \leq 10$, the fit yields $X_h = 0.0747(5)$, in good agreement with $X_h^{(r)}(g=5) = 3/40$ in Table I.

As discussed in Sec. II, we expect that an unstable geometric-cluster fixed point occurs in the range $0 < p_g < p_r$ for the tricritical Blume-Capel model. This is clearly shown by Fig. 4, indicating $p_g \approx 0.62$. Thus, we performed extensive simulations in the range $0.61 \leq p \leq 0.65$, and the system sizes were taken as $8 \leq L \leq 160$. We fitted Eq. (13) to the Monte Carlo data of r . After a cutoff for small system sizes $L \leq 12$, we obtain $p_c = 0.6227(1)$ and $y_p = 0.4254(6)$, where the statistical error bars are two standard deviations in the fit. The value of y_p is in good agreement with the expected value $y_p = 2 - X_p = 17/40$ (Table I).

At the geometric-cluster fixed point p_g , Table I predicts $X_h^{(g)}(g=5) = 21/160$. Thus, we fitted the following equation to the data of S_2 near p_g :

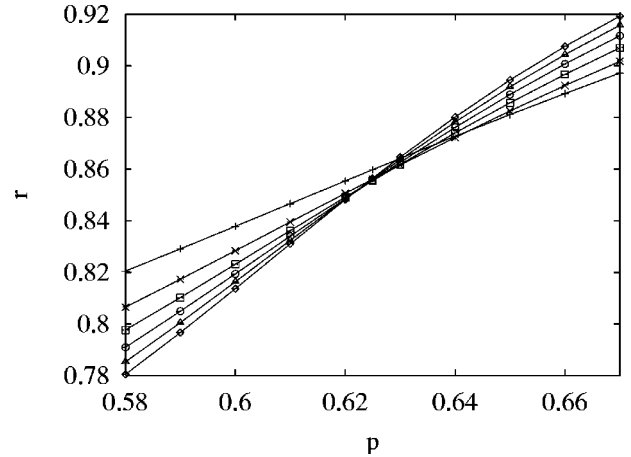


FIG. 4. The dimensionless ratio r near the geometric-cluster fixed point p_g for the tricritical Blume-Capel model. The data points $+$, \times , \square , \circ , \triangle , and \diamond represent $L=8, 12, 16, 20, 24$, and 28 , respectively.

$$S_2 = L^{-2X_h^{(g)}} [s_0 + s_1(p - p_c)L^{y_p} + s_2(p - p_c)^2 L^{2y_p} + \dots + s_6(p - p_c)^6 L^{6y_p} + b_1 L^{y_1} + b_2 L^{y_2} + b_3 L^{y_3} + c_1(p - p_c)L^{y_1 + y_p} + n_1(p - p_c)^2 L^{y_p}]. \quad (15)$$

Again, the exponents for finite-size corrections were simply taken as $y_1 = -1$, $y_2 = -2$, and $y_3 = -3$. After a cutoff for small systems $L \leq 12$, we obtain $p_c = 0.62265(10)$ and $X_h^{(g)} = 0.1311(5) \approx 21/160 = 0.13125$.

For the general Blume-Capel model described by Eq. (9), the RG flows should, in principle, be shown in the three-parameter space (p, K, D) . For simplicity, we only consider its projection onto the plane (p, K) , which is schematically shown in Fig. 5. Areas $K < K_{tc}$ and $K > K_{tc}$ represent a critical sheet and a region for first-order phase transitions, respectively. For $K \rightarrow \infty$, the percolation problem of this Blume-Capel model reduces to the bond-percolation model [3,25], which has a percolation threshold is $p_c = 1/2$ on the square lattice. For $K < K_{tc}$, the whole area above the solid line, $p = 1 - \exp(-2K)$, at within the percolation thresholds, and critical properties are governed by the fixed point ‘‘P1,’’ in the universality class of the tricritical $q=1$ Potts model. Besides this, there are four other fixed points ‘‘I,’’ ‘‘TI,’’ ‘‘GT,’’ and ‘‘BP,’’ which represent the Ising, the tricritical Blume-Capel, p_g of the tricritical Blume-Capel, and the bond-percolation model, respectively. Arrows show the direction of the RG flows.

The tricritical $q=3$ Potts model. It has been known [3] that, by including vacancies in the pure Potts model (1), the tricritical Potts model can be obtained. The Hamiltonian of the tricritical $q=3$ Potts model on the square lattice reads

$$\mathcal{H}/k_B T = -K \sum_{\langle i,j \rangle} \delta_{\sigma_i, \sigma_j} (1 - \delta_{\sigma_i, 0}) - D \sum_k \delta_{\sigma_k, 0} \quad (\sigma = 0, 1, 2, 3). \quad (16)$$

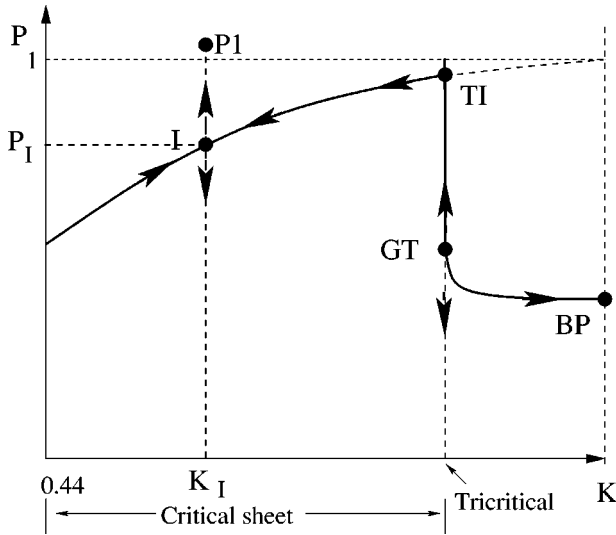


FIG. 5. RG flows diagram of the Blume-Capel model in the plane (K, P) . The areas $K < K_{tc}$ and $K > K_{tc}$ represent a critical sheet and the region for first-order phase transitions, respectively. The model reduces to the bond-percolation model for $K \rightarrow \infty$, which has a percolation threshold “BP” at $p = 1/2$. There are in total five fixed points “I,” “P1,” “TI,” “GT,” and “BP,” representing the Ising, the tricritical $q=1$ Potts, the tricritical Blume-Capel, the geometric-cluster fixed point of the tricritical Blume-Capel, and the bond-percolation models, respectively. Arrows show the direction of the RG flows.

By means of a sparse transfer matrix technique, we have determined the tricritical points [19] as $K_{tc} = 1.649\,923(5)$, $D_{tc} = 3.152\,173(10)$, and $\rho_{tc} = 0.34\,572(5)$ for the vacancy density.

Analogously, during the Monte Carlo simulations, we fixed the total number of vacancies, and thus used a combination of the Wolff [26] and the geometric cluster [21,22] steps. The system sizes were taken as $8 \leq L \leq 160$, and periodic boundary conditions were applied. The sampled quantities include S_2 , S_4 , and a dimensionless ratio $Q = \langle S_2 \rangle^2 / \langle 3S_2^2 - 2S_4 \rangle$. Compared to the aforementioned ratio r , the quantity Q is more in line with the well-known Binder ratio [24]. Near the random-cluster fixed point $p_r = 1 - \exp(-K_{tc}) \approx 0.808$, the Monte Carlo data of Q also reveal that the bond-dilution scaling field is irrelevant.

Figure 6 shows parts of the Monte Carlo data of Q in the range $p < p_r$, and indicates the geometric-cluster fixed point $p_g \approx 0.64$. According to the least-square criterion, we fitted Eq. (13) to the data of Q in the range $0.62 \leq p \leq 0.66$. The value of y_p is fixed at $2 - 2X_r = 25/84$ (Table I), we obtain $p_g = 0.6395(2)$, with two standard deviations for the error bar.

We illustrate the data for S_2 at $p_g = 0.6395(2)$ in Fig. 7 versus $L = L^{-15/66}$. The approximate linearity indicates that $X_h^{(g)} = 15/112$, as predicted in Table I. Moreover, we fitted Eq. (15) to the data of S_2 . After a cutoff for small system sizes $L \leq 12$, we obtain $X_h^{(g)} = 0.1337(6)$, in good agreement with $X_h^{(g)} = 15/112$.

The dilute $q=4$ Potts model. The $q=4$ Potts model is a marginal case, not only because the second-leading thermal

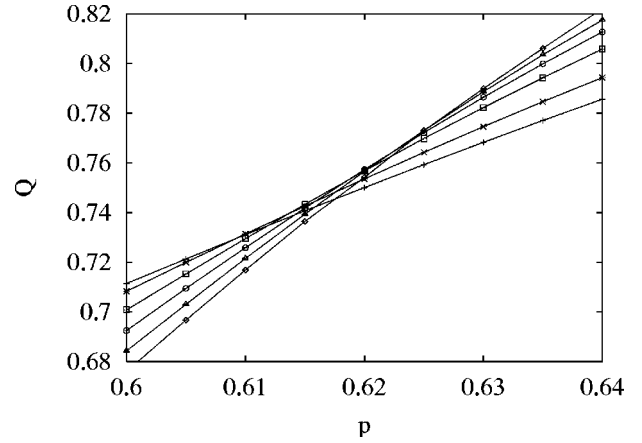


FIG. 6. The dimensionless ratio Q near the geometric-cluster fixed point p_g for the tricritical $q=3$ Potts model. The data points $+$, \times , \square , \circ , \triangle , and \diamond represent $L=12, 16, 24, 32, 40$, and 48 , respectively.

scaling field is marginal $y_{t2}=0$ [6,7], but also the bond-dilution exponent $y_p=0$. We investigate a dilute $q=4$ Potts model Eq. (16) at a point where the second-leading thermal field vanishes. By means of the transfer matrix technique, we have determined this point [19] as $K_c = 1.45\,790(1)$, $D_c = 2.478\,438(2)$, and $\rho_c = 0.21\,207(2)$ for the vacancy density. Analogously, the Monte Carlo simulations use a fixed-vacancy-density ensemble. Periodic boundary conditions were applied, and the system sizes were taken in the range $8 \leq L \leq 280$. At the random-cluster fixed point p_r , we find that Eq. (14) is sufficient to describe the data of S_2 , and finite-size corrections decay very rapidly with the leading exponent $y_1 = -2.3(2)$. Furthermore, the fit yields that the magnetic exponent $X_h = 0.1248(3)$, in good agreement with $X_h = 1/8$. This indicates that, as expected, logarithmic corrections due to the marginal second-leading thermal field are absent for the dilute $q=4$ Potts model at this point. For Potts clusters ($p=1$), we find that the data of S_2 cannot be described by Eq. (14) anymore. Instead, we used the following equation during the numerical fit:

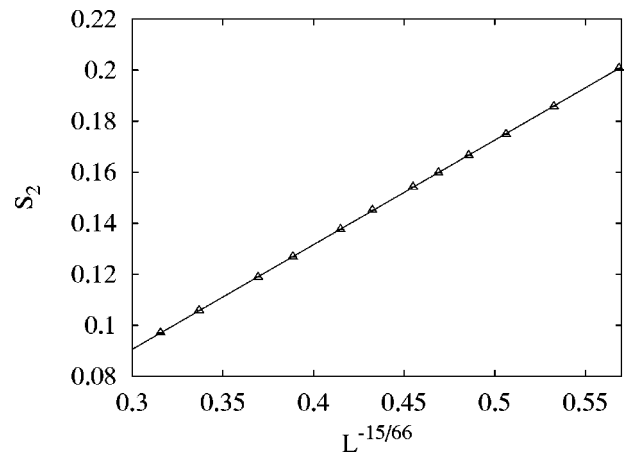


FIG. 7. The quantity S_2 at the geometric-cluster fixed point p_g for the tricritical $q=3$ Potts model vs $L^{-2X_h^{(g)}} = L^{-15/66}$. The system sizes are in the range $12 \leq L \leq 160$.

TABLE II. The hull-cluster scaling dimensions X_H for the critical and the tricritical Potts model in two dimensions. The superscripts (r) and (g) represent the random- and the geometric-cluster fixed point, p_r and p_g , respectively.

	Critical Potts model					Tricritical Potts model				
q	0	1	2	3	4	3	2	1	0	
$X_H^{(r)}$	0	1/4	1/3	2/5	1/2	4/7	3/5	5/8	2/3	
$X_H^{(g)}$	3/4	2/3	5/8	7/12	1/2	5/12	3/8	1/3	1/4	

$$S_2 = L^{-2X_h}(a_0 + a_1/\ln L + a_2/\ln^2 L + a_3L^{-2}). \quad (17)$$

This reflects that, for the $q=4$ Potts model, the bond-dilution scaling field is indeed marginal.

IV. DISCUSSION

We have determined geometric properties of the general critical and tricritical Potts models in two dimensions. Apart from the random-cluster fixed point p_r , we find a geometric-cluster fixed point p_g . Moreover, on the basis of the theory of the Coulomb gas, we predict critical exponents near p_g , which include the magnetic, the thermal, and the bond-dilution exponents, shown in Table I. We have performed extensive Monte Carlo simulations, and confirmed some predictions. As another example, we consider the fractal dimension of the hull or external perimeter of a cluster, which consists of all the absent bonds surrounding the cluster of interest. For the critical Potts model, exact values of the hull-cluster scaling dimension $X_H^{(r)}$ near the random-cluster fixed point p_r have already been given [17] as

$$X_H^{(r)} = (g - 2)/g, \quad (18)$$

with g being the coupling constant. By assuming that this formula applies to the tricritical branch of the Potts model, and according to the relation $gg' = 16$ between the fixed points p_r and p_g , we obtain near the geometric-cluster fixed point p_g

$$X_H^{(g)} = (8 - g)/8. \quad (19)$$

The values of $X_H^{(r)}$ and $X_H^{(g)}$ for integers $0 \leq q \leq 4$ are listed in Table II.

From Table I, the geometric-fixed point p_g of the bond-percolation model corresponds to p_r of the tricritical $q=0$ Potts model.

ACKNOWLEDGMENTS

The authors are indebted to Dr. J.R. Heringa and X.F. Qian for valuable discussions. This research was supported by the Dutch FOM foundation (“Stichting voor Fundamenteel Onderzoek der Materie”) which is financially supported by the NWO (“Nederlandse Organisatie voor Wetenschappelijk Onderzoek”).

[1] M.E. Fisher, *Physics* (N.Y.) **3**, 25 (1967).
 [2] R.B. Potts, *Proc. Cambridge Philos. Soc.* **48**, 106 (1952).
 [3] F.Y. Wu, *Rev. Mod. Phys.* **54**, 235 (1982).
 [4] P.W. Kasteleyn and C.M. Fortuin, *J. Phys. Soc. Jpn.* **46** (Suppl.), 11 (1969); C.M. Fortuin and P.W. Kasteleyn, *Physica* (Amsterdam) **57**, 536 (1972).
 [5] A. Coniglio and F. Peruggi, *J. Phys. A* **15**, 1873 (1982).
 [6] B. Nienhuis, *J. Phys. A* **15**, 199 (1982).
 [7] B. Nienhuis, *Phase Transitions and Critical Phenomena*, edited by C. Domb and J.L. Lebowitz (Academic Press, London, 1987), Vol. 11, p. 1, and references therein.
 [8] A.A. Belavin, A.M. Polyakov, and A.B. Zamolodchikov, *J. Stat. Phys.* **34**, 763 (1984); *Nucl. Phys. B* **241**, 333 (1984); D. Friedan, Z. Qiu, and S. Shenker, *Phys. Rev. Lett.* **52**, 1575 (1984).
 [9] J.L. Cardy, in *Phase Transitions and Critical Phenomena*, edited by C. Domb and J.L. Lebowitz (Academic Press, London, 1987), Vol. 11, p. 55, and references therein.
 [10] A.L. Stella and C. Vanderzande, *Phys. Rev. Lett.* **62**, 1067 (1989).
 [11] B. Duplantier and H. Saleur, *Phys. Rev. Lett.* **63**, 2536 (1989).
 [12] C. Vanderzande, *J. Phys. A* **25**, L75 (1992).
 [13] H.W.J. Blöte, Y.M.M. Knops, and B. Nienhuis, *Phys. Rev. Lett.* **68**, 3440 (1992).
 [14] M. Blume, *Phys. Rev.* **141**, 1517 (1966).
 [15] H.W. Capel, *Physica* (Amsterdam) **32**, 966 (1966); **33**, 295 (1967).
 [16] A. Coniglio and W. Klein, *J. Phys. A* **12**, 2775 (1980).
 [17] A. Coniglio, *Phys. Rev. Lett.* **62**, 3054 (1989).
 [18] L. Onsager, *Phys. Rev.* **65**, 117 (1944).
 [19] X.F. Qian, Y. Deng, and H.W.J. Blöte (unpublished).
 [20] P.D. Beale, *Phys. Rev. B* **33**, 1717 (1986).
 [21] J.R. Heringa and H.W.J. Blöte, *Physica A* **232**, 369 (1996).
 [22] J.R. Heringa and H.W.J. Blöte, *Phys. Rev. E* **57**, 4976 (1998).
 [23] R.H. Swendsen and J.S. Wang, *Phys. Rev. Lett.* **62**, 163 (1989).
 [24] K. Binder, *Z. Phys. B: Condens. Matter* **43**, 119 (1981).
 [25] D. Stauffer and A. Aharony, *Introduction to Percolation Theory* (Taylor & Francis, Philadelphia, 1994).
 [26] U. Wolff, *Phys. Rev. Lett.* **62**, 361 (1989).